Solid State Ionics 180 (2009) 805–811

Contents lists available at ScienceDirect

Solid State Ionics

journal homepage: www.elsevier.com/locate/ssi

Cathode-supported micro-tubular SOFCs based on $Nd_{1.95}NiO_{4+\delta}$: Fabrication and characterisation of dip-coated electrolyte layers

Henning Luebbe [a,b,*], Jan Van herle [a], Heinrich Hofmann [b], Paul Bowen [b], Ulrich Aschauer [b], Andreas Schuler [b], Frans Snijkers [c], Hans-Juergen Schindler [d], Ulrich Vogt [d], Cécile Lalanne [e]

[a] Ecole Polytechnique Fédérale de Lausanne, STI-IGM, Industrial Energy Systems Laboratory (LENI), Station 9, CH-1015 Lausanne, Switzerland
[b] Ecole Polytechnique Fédérale de Lausanne EPFL, STI-IMX, Powder Technology Laboratory, Station 12, CH-1015 Lausanne, Switzerland
[c] Vlaamse instelling voor technologisch onderzoek VITO, Boeretang 200, BE-2400 Mol, Belgium
[d] Eidgenössische Materialprüfanstalt EMPA, Hochleistungskeramik, Ueberlandstrasse 129, CH-8600 Duebendorf, Switzerland
[e] CNRS, Université de Bordeaux, ICMCB, 87 avenue du Dr. A. Schweitzer, Pessac, F- 33608, France

ARTICLE INFO

Article history:
Received 19 September 2008
Received in revised form 5 January 2009
Accepted 5 January 2009

Keywords:
Micro-tubular SOFC
Cathode-supported cell (CSC)
Nickelate oxide
Colloidal stability
Cosintering

ABSTRACT

Fabrication conditions to obtain dense electrolyte double layers on a porous micro-tubular cathode substrate were investigated. Porous tubes of a nickelate material, $Nd_{1.95}NiO_{4+\delta}$, were fabricated by cold-isostatic pressing (CIP) and sintering. Thin films of electrolyte powders $Ce_{0.9}Gd_{0.1}O_{1.95}$ (GDC) and $Zr_{0.89}Sc_{0.1}Ce_{0.01}O_{1.95}$ (SSZ) were applied by dip-coating in aqueous suspensions. Electrolyte powders had been attrition-milled to decrease their particle size and densification temperature. The quantity of polyacrylic acid (PAA) as dispersant was optimised by ζ-potential measurements. The densification behaviour was studied by dilatometry and SEM-imaging. A sintering temperature of 1250 °C was found to densify GDC whereas SSZ-layers remained slightly porous.

1. Introduction

Solid oxide fuel cells (SOFC) are energy conversion devices that convert chemical energy of a fuel directly into electricity and useful heat, where the latter is recovered at the device's high working temperature. The two principal setups for SOFC are the planar and tubular configurations. Both of them possess advantages and disadvantages in their design. Planar fuel cells can be produced more cost-efficiently and show higher power densities than tubular SOFC, which in turn are easier to seal and resist better to thermal cycling. Furthermore, tubular fuel cells produced by Siemens-Westinghouse have demonstrated stable operation during >65,000 h which was never reported for planar SOFC. However, both designs suffer from relatively long start-up times (hours) which render the application in mobile power generation systems impractical.

Kilbride [1] has fabricated electrolyte-supported tubular SOFC with a diameter of 2.4 mm and lengths of 4 mm–100 mm (called micro-tubular SOFC to point out the difference to Siemens-Westinghouse with tubes of ca. 22 mm inner diameter and 1500 mm length) that were thermally cycled between 20 and 900 °C up to 53 times with heating and cooling rates of 100 K/min without any sign of cell performance degradation due to thermal cycling. As the cells can endure thermal stresses, the gas manifold could be realised in the cold zone where conventional low-cost materials are applicable.

In recent years, researchers have prepared micro-tubular cells with electrolyte, anode and cathode supports. Electrolyte-supported cells (ESC) were reported by Sammes [2]. When the electrolyte thickness was reduced from 550 to 220 μm, an increase of maximum power density of 30% was observed, indicating the importance of the contribution of ohmic resistance to the overall performance. Maximum power densities of LSGM-based tubes amounted to 482 mW/cm^2 at 800 °C for 220 μm-thick electrolyte tubes.

Anode-supported cells (ASC) were reported by Nguyen [3], Sarkar [4], Funahashi [5] and Suzuki [6]. Maximum power outputs reached up to 1017 mW/cm^2 at 550 °C [6]. ASC are advantageous for electrolyte densification, as the employed sintering temperature of ca. 1400 °C is sufficiently high to densify commonly used electrolytes such as YSZ, and for lowering the ohmic resistance, as the electrolyte thickness is in the range of 5–20 μm. Nevertheless, problems can arise from cathode current collection, redox-instability of the anode and fuel utilisation limitations (due to the thick anode).

Reports on micro-tubular cathode-supported cells (CSC) are sparse, which can in part be attributed to the difficulties of preparing a dense electrolyte on a porous cathode at reduced sintering temperature. Yamaguchi [7] has reported CSC consisting of a ca. 400 μm thick LSM-support with a GDC/SSZ bilayer electrolyte. The maximum power densities achieved were 73 mW/cm^2 and 230 mW/cm^2 at 600 and

* Corresponding author. EPFL STI IMX LTP, MXC 319 (Bâtiment MXC), Station 12, CH-1015 Lausanne, Switzerland. Tel.: +41 21 6936888; fax: +41 21 6933089.
E-mail address: henning.luebbe@epfl.ch (H. Luebbe).

0167-2738/$ – see front matter © 2009 Elsevier B.V. All rights reserved.
doi:10.1016/j.ssi.2009.01.010

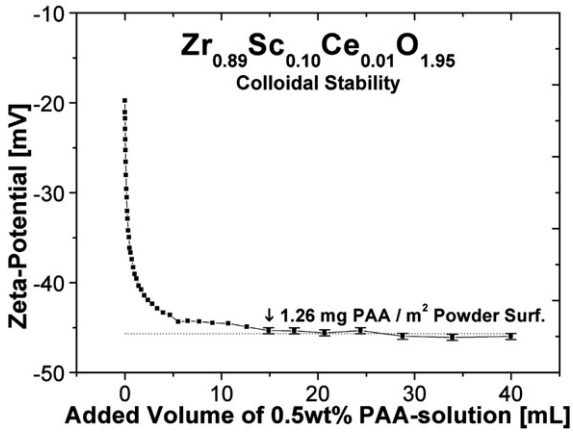

Fig. 1. ζ-Potential measurement of aqueous SSZ-suspension titrated with PAA-solution. The pH of the suspension and the solution was 9.5. The determined volume of PAA-solution was recalculated to yield the coverage of mass PAA per SSZ particle surface area using the Specific Surface Area (SSA) of SSZ.

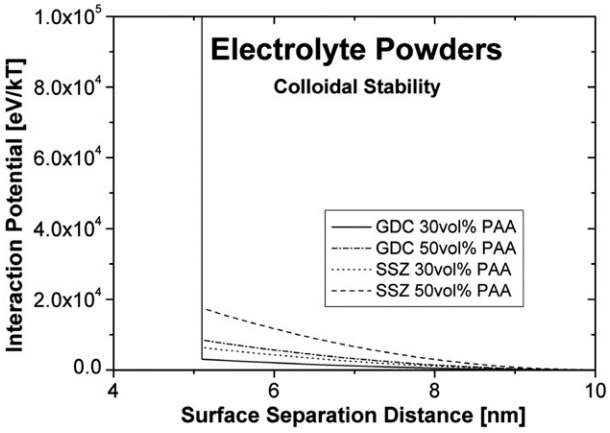

Fig. 2. Interaction Potential between the respective electrolyte powder particles. The potential wall at ca. 5 nm due to adsorbed PAA-molecules prevents agglomeration of the particles. Parameters for the calculations are shown in Table 1.

700 °C respectively. The formation of an unknown reaction phase of low ionic conduction at the GDC/SSZ interface was observed after sintering at 1300 °C. It was believed that with the further reduction of sintering temperature the reaction of GDC and SSZ can be avoided. Liu reported performances of $La_{0.6}Sr_{0.4}Co_{0.2}Fe_{0.8}$ (LSCF)/GDC tubes with electrolyte and anode layers, either subsequently sintered [8] or cofired [9]. GDC was used in both cases as single electrolyte layer and densified at 1200 °C. Maximum power densities amounted to 160 mW/cm^2 and 90 mW/cm^2 at 600 °C for subsequently sintered and cosintered electrolyte/anode respectively. Like Yamaguchi [7], this work also pursues the fabrication of a bilayer electrolyte. Advantages, challenges and the necessity of using thin zirconia in conjunction with thin ceria had been reported before [10,11].

Nickelates of the general formula $A_2NiO_{4+\delta}$ have demonstrated to possess superior oxygen transport properties over commonly used cathode materials, namely LSCF and LSM. It was shown [12] that the oxygen diffusion coefficient in $La_2NiO_{4+\delta}$ is substantially higher than in LSCF (ca. 1 order of magnitude at 700 °C). In another study [13], the variation of cations on the A-side (La, Pr, Nd) indicated that under-stochiometric $Nd_{1.95}NiO_{4+\delta}$ shows more promising properties for application as a cathode material. The oxygen surface exchange coefficient at 700 °C with this composition was 1 order of magnitude higher than with LSCF and differed from the values measured by Skinner [12], which was attributed to attrition milling leading to different particle morphologies. Exact values of oxygen diffusion coefficients and surface exchange coefficients for $Nd_{1.95}NiO_{4+\delta}$ were recently published by Lalanne [14]. Mauvy et al. [15] measured ASRs (area specific resistances, Ω cm^2) of micro-cathodes in contact with YSZ pellets for $Nd_2NiO_{4+\delta}$ and LSM. At 700 °C, the ASR with nickelate was ca. 1 order of magnitude lower than that with LSM. However, reports on complete (planar) cells with nickelate cathodes are rare [14,16], and have not been reported for micro-tubular SOFC. It is the aim of this work to demonstrate the feasibility of the fabrication of cathode-supported micro-tubular SOFC based on nickelate tubes.

Table 1
Summary of parameters used in the calculations.

	$\rho_{th.}$ [g/cm^3]	ζ-pot. [mV]	A_H [J]	a [nm]	ϕ_2	χ	I_c [mol/l]	δ [nm]
GDC	7.24	−20	10^{-20}–10^{-19}	90	0.3–	0.35	10^{-3}	5
SSZ	5.95	−45	$7*10^{-20}$	185	0.5			

$\rho_{th.}$ represents the theoretical density. The ζ-potential used was derived from measurements as presented in Fig. 1 for pH = 9.5. The Hamaker-constant for GDC was not found and therefore varied in the given range. The value for A_H of SSZ was taken from Bergstrom [29] and was assumed to be the same as for 3YSZ. The values for a were taken from Table 2. The value χ for PAA/water interaction is 0.35 [23]. At pH = 9.5, PAA-molecules are elongated [18], which, for molecular weight 2000, equals δ ca. 5 nm.

2. Experimental

2.1. Tube shaping

Nickelate powder of the composition $Nd_{1.95}NiO_{4+\delta}$ was fabricated by Marion Technologies, France, and characterised at ICMCB, France. The nickelate powder had a particle size of 0.88 µm ($d_{v,50}$), a specific surface area of 4.4 m^2/g and a molar ratio of Nd/Ni of 1.966 ± 0.009 (measured by ICP). The shaping of tubes was performed at VITO, Belgium. Powder mixtures of 98 g of nickelate and 6 g rice starch (Remyline AX-DR, Remy Industries, Belgium) as pore former were homogenised by mixing in 150 ml acetone in a planetary ball mill with a polymer jar and YSZ milling media for 3 min. After milling, the acetone was evaporated and the dry powder mixture sieved over a 500 µm mesh. The powder was compacted by cold isostatic pressing (CIP) in a tubular rubber mould at 80 MPa. The green tubes were calcined by heating up with 30 °C/h to 500 °C, followed by a dwell of 1 h, heating up with 100 °C/h to the presintering temperature of 1060 °C. After 4 h of dwell, cooling down to room temperature occurred at a rate of 150 °C/h. Presintered tubes had an inner diameter of 4.9 ± 0.1 mm, wall thickness of 1 ± 0.1 mm and were cut to lengths of 50 mm.

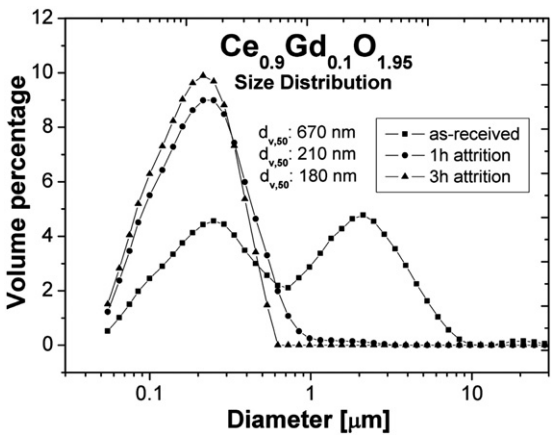

Fig. 3. PSD of as-received and attrition-milled GDC given in volumetric percentage.

2.2. Powders and suspensions

Commercial $Ce_{0.9}Gd_{0.1}O_{1.95}$ (Nextech, Lot-Nr.159-64, hereafter called GDC) and $Zr_{0.89}Sc_{0.1}Ce_{0.01}O_{1.95}$ (Praxair, Lot-Nr. 03-P5978BM, hereafter called SSZ) powders were used. Anode powder mixtures of 60wt.% NiO (J.T. Baker)/40 wt.% 8YSZ (Tosoh) were prepared at SOFC power, Italy. Attrition milling of electrolyte and anode powders was performed in an attritor at 1500 rpm with commercial 3YSZ grinding spheres of 1.25 mm diameter (Tosoh) to decrease the particle size and densification temperature of the electrolyte and to homogenise the particle size of the anode powder mixture. Polyacrylic acid (PAA) of molecular weight 2000 was used as a dispersant; the pH of aqueous PAA-solutions was adjusted to 9.5 by adding aqueous solution of NH_4OH, the molar ratio NH_4OH/PAA was 1.5. The necessary amount of PAA to stabilise the particles was determined by titrating aqueous powder suspensions in 10^{-3} M KNO_3 with aqueous PAA-solution (both set to pH = 9.5) while measuring the ζ-potential. The particle size distribution (PSD) of attrition-milled and as-received electrolyte and anode powder suspensions was measured by Laser Diffraction on a Malvern Mastersizer S.

2.3. Dilatometry and densification

Shrinkage of cathode-tubes and pellets of electrolyte and anode powders were measured by dilatometry at EMPA, Switzerland. Pellets of the respective powders were prepared by slip-casting aqueous powder suspensions. The shrinkage of cathode tubes in the pressed, green state was measured in tube axis direction. The shrinkage was investigated between 20 and 1400 °C with a heating rate of 5 K/min on a BAEHR Dil802 dilatometer. Densities of sintered pellets were measured by the Archimedes method. SEM images were recorded on cross-sections of fractured sintered pellets on a Philips XL 30 microscope.

2.4. Dip-coating and sintering

Presintered nickelate tubes were used as support for dip-coating. Suspensions of nickelate, electrolyte and anode powders with various concentrations between 5 and 25 wt.% solids were prepared for the tests. An aqueous solution of commercial polyvinylalcohol (PVA, Mowiol 3-96 from Kuraray Specialities Europe) was used to add a binder to the respective suspension. The amount of added PVA was 5 wt.% of the powder mass in suspension. The open-ended cathode tubes were fixed and sealed with a self-made device and sequentially dipped in nickelate-, electrolyte- and anode suspensions. The nickelate layer was needed to cover the macropores of the cathode tubes in order to avoid pinholes in the electrolyte layers. Explanations

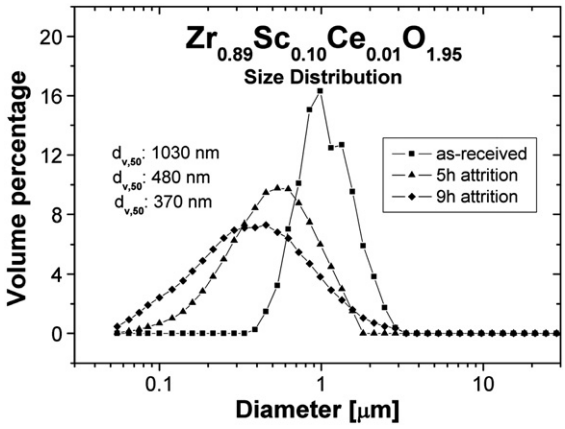

Fig. 4. PSD of as-received and attrition-milled SSZ given in volumetric percentage.

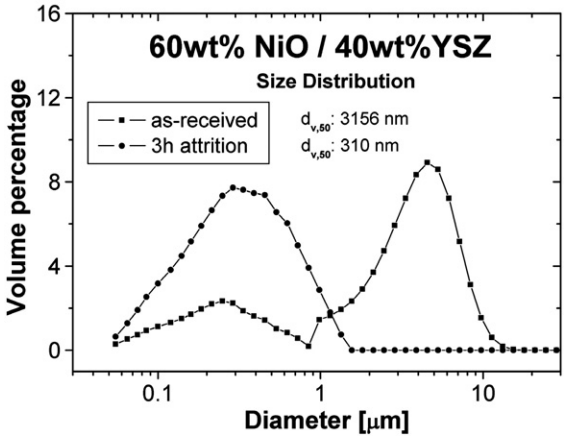

Fig. 5. PSD of as-received and attrition-milled SSZ given in volumetric percentage. In as-received state, NiO-particles had a size of ca. 5 μm.

therefore are given in Section 3.3. The tube withdrawal speed from the respective suspension was in the range of 60–90 mm/min. Dip-coated tubes were dried at 25 °C and 90% relative humidity for 24 h after each applied layer before the next layer was deposited. After the coating and drying process of tubes was completed, the coated tubes were sintered in a Nabertherm furnace with the following program: ramp to 400 °C at 30 K/h, 5 h dwell at 400 °C, ramp to 1250 °C at 50 K/h, 2 h dwell at sintering temperature, ramp to RT at 100 K/h.

3. Results and discussion

3.1. Colloidal properties of electrolyte and anode powders

In order to define the pH-value and determine the necessary amount of PAA-dispersant that is needed to stabilise the particles in suspension after attrition milling, ζ-potential measurements were carried out. Suspensions of electrolyte powder in aqueous 10^{-3} M KNO_3 solution were titrated with PAA-solution of known concentration. The ζ-potential of electrolyte powder suspensions with added PAA was measured over a pH-range from 4–12 by adjusting the pH with 1 M KOH and 1 M HNO_3. The ζ-potential was negative over the entire studied pH-range and its absolute value increased with the pH due to deprotonisation of PAA. Basic conditions of pH = 9.5 were chosen for the further work in order to increase the repulsive forces between particles. In addition, dopants of ZrO_2 are known to dissolve in strongly acidic conditions [17]. Furthermore, the state of PAA-molecules as dispersant is well-studied at different pH-values and shows brush-like configuration at basic conditions [18] which enhances the particle repulsion by adding a steric contribution.

The result of ζ-potential measurements during titration experiments of SSZ powder is presented in Fig. 1. Afterwards, calculations on the

Table 2
Summary of powder particle characteristics of electrolyte and anode materials in as-received state and after attrition.

	GDC		SSZ		NiO–8YSZ	
	As-received	3 h attrition	As-received	9 h attrition	As-received	3 h attrition
$d_{v,50}$ [nm]	670	180	1030	370	3156	310
Span	4.3	1.5	1.2	2.4	114.1	2.1
SSA [m^2/g]	16.9	24.7	11.8	22.5	2.4	8.2
F_{AG}	13.1	5.1	9.9	6.8	15.5	2.7

Span = $(d_{v,90} - d_{v,10})/d_{v,50}$. The factor of agglomeration F_{AG} equals $d_{BET}/d_{v,50}$ and represents the state of agglomeration of powder where smaller values mean lower agglomeration. $d_{BET} = 6/(SSA * \rho_{th})$ [μm].

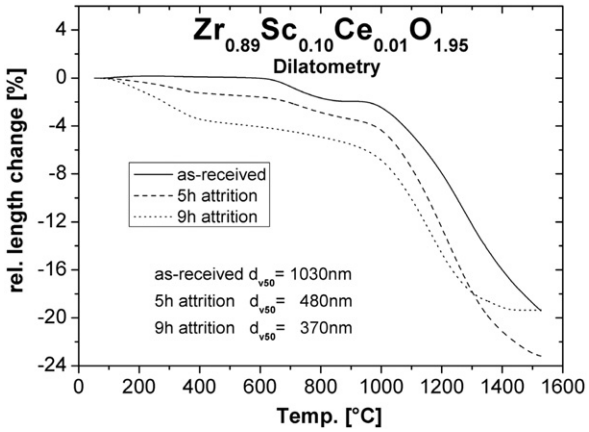

Fig. 6. Dilatometric measurements on slip-casted pellets of different SSZ powder suspensions. Differences in the overall shrinkage can be attributed to different green densities.

colloidal stability of particle suspensions were made using an in-house developed software code (Hamaker, available on the laboratory's web page [19]). The software calculates the particle interaction potential as a function of particle surface separation distance. The particle interaction potential is the sum of attractive van der Waals and repulsive interaction potentials due to steric and electrostatic contributions as shown in Eq. (1).

$$\Delta G_{int.} = \Delta G_{Attr.} + \Delta G_{Elec.} + \Delta G_{Ster.} \tag{1}$$

For the attractive interaction potential of 2 spheres of equal size with radius a, whose surfaces are separated by the distance s, the Gregory equation

$$\Delta G_{Attr.} = -\left(\frac{A_H \cdot a}{12s}\right)\left[1 - \frac{bs}{\lambda_0}\ln\left(1 + \frac{\lambda_0}{bs}\right)\right] \tag{2}$$

is valid in the size range of 100–1000 nm as retardation effects are taken into account [20,21]. The parameters b and λ_0 amount to 5.32 and 100 nm respectively. The former is a correction factor for retardation effects whereas the latter represents the characteristic wavelength for molecular motion. A_H is the effective Hamaker-constant.

The electrostatic contribution $\Delta G_{Elec.}$, according to the Hogg–Healy Fuerstenau approach [22] for 2 particles of equal size which is used in this work, is presented in Eq. (3).

$$\Delta G_{Elec.} = \pi \cdot \varepsilon \cdot \varepsilon_0 \cdot \frac{a}{2}\left[(\psi_1 + \psi_2)^2 \ln(1 + \exp(-\kappa \cdot s)) + (\psi_1 - \psi_2)^2 \ln(1 - \exp(-\kappa \cdot s))\right] \tag{3}$$

The electric permittivity of vacuum is labelled ε_0 and the relative electric permittivity of the suspending medium is ε. The surface potential of particle i is labelled ψ_i in Eq. (3). It is calculated from the experimentally accessible ζ-potential by

$$\psi(r) = \frac{2k_B T}{ze} \ln\left[\frac{1 + \left(\frac{\exp\left(\frac{ze\zeta}{2k_B T}\right) - 1}{\exp\left(\frac{ze\zeta}{2k_B T}\right) + 1}\right)\exp(-\kappa(r - d_s))}{1 - \left(\frac{\exp\left(\frac{ze\zeta}{2k_B T}\right) - 1}{\exp\left(\frac{ze\zeta}{2k_B T}\right) + 1}\right)\exp(-\kappa(r - d_s))}\right] \tag{4}$$

where r is the distance from the particle surface and d_s is the thickness of the Stern layer. The Boltzmann constant is represented by k_B. The electron charge is e and its quantity is z. In the case of water as solvent, $\varepsilon\varepsilon_0 = 6.954 * 10^{-20}$ C^2 J^{-1} m^{-1} and $d_s = 0.5$ nm.

The thickness of the double layer according to Debye–Hückel theory is κ^{-1}. It can be calculated by

$$\kappa^{-1} = \sqrt{\frac{\varepsilon\varepsilon_0 k_B T}{2e^2 I_c N_A}} \tag{5}$$

where N_A is the Avogadro number and I_c represents the ionic concentration.

For steric contribution, the expression by Bergstrom [23] used in this work reads

$$\Delta G_{Ster.} = \frac{\pi \cdot a \cdot k_B T}{\bar{V}} \phi_2^2 \left(\frac{1}{2} - \chi\right)(2\delta - s)^2 \tag{6}$$

In this equation, $\bar{V}$ is the molar volume of the solvent, ϕ_2 is the volume fraction of polymer in the adsorbed layer and χ is a measure for solvent–adsorbate interactions.

The thickness of the adsorbed surface layer is given by δ and the absolute temperature in Kelvin is given by T.

All the parameters used in the calculation are shown in Table 1. The results of the interaction potential calculations for SSZ and GDC powders are shown in Fig. 2. The interaction potential shows a very steep increase at ca. 5 nm which leads to a potential "wall" between particles that prevents their agglomeration. It originates mostly from the fact that elongated PAA-molecules of molecular weight 2000 have a length of ca. 5 nm. The total volume of the surface layer is given by the length of the adsorbed PAA-molecules on the particle surface and the volume fraction of PAA molecules ϕ_2 in this layer is given by the volume of PAA-chains with respect to the total volume of the adsorbed surface layer. Since this parameter is experimentally not accessible, ϕ_2 was varied in the calculations between 30 and 50 vol.%. The adsorbed PAA-molecules can be considered as monosized discs, whose density in the random close packed state amounts to 54% [18]. Since charged PAA-molecules repel each other electrostatically, the selected range of ϕ_2 of 0.3–0.5 is reasonable. The polymer volume fraction ϕ_2 influences the slope of the particle interaction energy curve at distances between the potential "wall" at ca. 5 nm and a distance of 9–10 nm. These calculations confirmed that the colloidal suspensions are stable as no attractive minimum was predicted.

3.2. Densification of electrolyte and anode powders

The PSD of as-received and attrition-milled GDC is shown in Fig. 3. Soft agglomerates of the as-received powder were not found anymore in the attrition-milled powder even after milling times as low as 1 h. After milling for longer than 1 h, the PSD showed only marginal differences; therefore the attrition was stopped after 3 h.

The PSD of as-received and attrition-milled SSZ is shown in Fig. 4. SSZ is much harder than GDC and needed consequently longer attrition times. After 9 h, no further decrease of the particle size occurred and the attrition was stopped.

The influence of attrition-milling on the PSD of anode powder mixture is shown in Fig. 5. The anode powder was attrition-milled as the PSD of as-received powder mixture was bi-modal with modes at 250 nm and 5 μm. After passing a suspension of the as-received powder through a 1 μm-filter, the greenish color changed to white

Table 3
Densities of sintered pellets of the respective attrition-milled powder.

Density in % of ρ_{th}	SSZ		GDC
	5 h attrition	9 h attrition	3 h attrition
$T_{Sint} = 1200$ °C	80	89	94
$T_{Sint} = 1250$ °C	83	90	97
$T_{Sint} = 1300$ °C	84	93	95

Measurements were performed using the Archimedes method.

Table 4
Reported values for TECs of utilised materials.

	$Nd_2NiO_{4+\delta}$	GDC	SSZ	NiO/YSZ
TEC (10^{-6} K^{-1})	12.7 [13]	ca. 11 [27]	9–10 [24]	12.2 [28]

The TEC of $Nd_2NiO_{4+\delta}$ is a mean value between 20 and 1000 °C. The TEC of GDC is a mean value between 20 and 600 °C. The TEC of $Zr_{0.92}Y_{0.08}O_{1.96}$ at 600 °C according to Hayashi [24] is 10.1, the TEC of SSZ is not known and must therefore be estimated (cf. Section 3.2). Montross [28] reported $12.2*10^{-6}$ K^{-1} for 30 vol.% Ni in Ni/YSZ.

which indicated that NiO-particles had a size of ca. 5 μm in the as-received state. This was confirmed by SEM analysis. All powder particle characteristics are summarised in Table 2.

The influence of attrition-milling on densification behaviour was measured by dilatometry and density measurements of pellets after sintering at various temperatures. Results of dilatometric measurements for SSZ are shown in Fig. 6.

The large differences in densification between samples after 5 h and 9 h of attrition milling indicate the importance of producing fine SSZ powders and therefore long attrition times. Differences in the overall shrinkage can be attributed to different green densities. Densities of pellets of 5 h and 9 h attrited SSZ and 3 h attrited GDC after different sintering temperatures are summarised in Table 3. In order to cosinter different layers, their thermal expansion coefficient (TEC) as well as their shrinkage behaviour has to be matched. Reported TECs of the different materials are presented in Table 4. Although there is a difference between electrode and electrolyte materials where the former possess greater TECs, the difference is small enough to expect mechanical compatibility, especially since thin layers, as the electrolytes, are able to cope with differences of TEC and deform slightly without forming cracks. Since there was no reported value for SSZ, its TEC had to be estimated. Hayashi [24] reported $10*10^{-6}$ K^{-1} for 10YSZ at 600 °C and decreasing TECs for increasing yttria doping content. Gorshkov [25] reported a TEC of $9.41*10^{-6}$ K^{-1} for $Zr_{0.835}Sc_{0.165}O_{2-\delta}$ between 40 and 850 °C. Therefore, a range of $9–10*10^{-6}$ K^{-1} seems plausible. However, the TEC of SSZ remains uncertain and will therefore be measured in the near future to state it more precisely.

The shrinkage behaviour of the cathode tubes and electrolyte and anode powder pellets is presented in Fig. 7. GDC and SSZ start densifying at lower temperatures than cathode and anode materials which induces tensile stresses in the electrolyte layers and can constrain their sintering. However, the sintering of electrolyte layers was found to be sufficient which is shown in Section 3.3. Presintered tubes showed shrinkages of roughly 12% when sintered at 1250 °C, which correlates well with the data in Fig. 7.

3.3. Tube substrates and densification of electrolyte layers

Only presintered tubes were used for subsequent processing. Green tubes disintegrated when they came in contact with aqueous suspensions during dip-coating. Thin films did not adhere well on completely sintered substrates due to the lack of capillary forces as small pores are no longer present on sintered substrates. Furthermore, fully sintered tubes do not further shrink during sintering of the coatings which constrains the densification of electrolyte layers.

SEM images of presintered tubes are shown in Fig. 8. Small pores (Fig. 8a) in the range of 5–10 μm as well as large pores (Fig. 8b) with a size of up to ca. 100 μm are visible. Whereas the former ones are possible to cover with electrolyte layers, the latter require thick layers to avoid the formation of pinholes. Investigations to optimise the pore size and its distribution are ongoing. In order to prepare complete cells, a nickelate layer, a layer of GDC and a layer of SSZ were sequentially dip-coated, dried and sintered. Dip-coated layers adhered well to the substrate due to capillary forces of small pores shown in Fig. 8a. The nickelate layer was needed to homogenise the rough surface and cover the big pores shown in Fig. 8b to avoid pinholes in

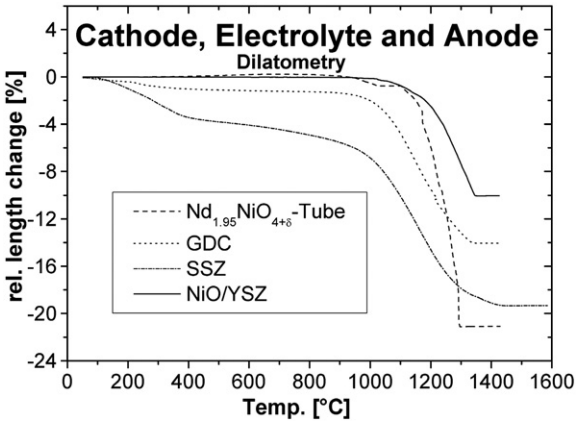

Fig. 7. Comparison of the shrinkage behaviour of the different materials used. The shrinkage of nickelate-tubes was measured in tube direction. GDC, SSZ and anode powders were attrited.

the electrolyte layers. Electrolytes have to be gas tight in order to separate the cathode and anode gas compartments. Pinholes in the electrolyte would endanger the cell's gas tightness. Fig. 9a shows a cross-section of the sequentially deposited nickelate-, GDC- and SSZ-layers in the dried green state before sintering. After sintering at 1250 °C for 2 h, a dense GDC microstructure (Fig. 9b) was observed, whereas the SSZ-layer maintained some porosity (Fig. 9c and d). These observations correlate well with the measured densities of sintered pellets (Table 3). Yamaguchi [26] prepared micro-tubular ASC with a GDC electrolyte and stated that substrate shrinkages of at least

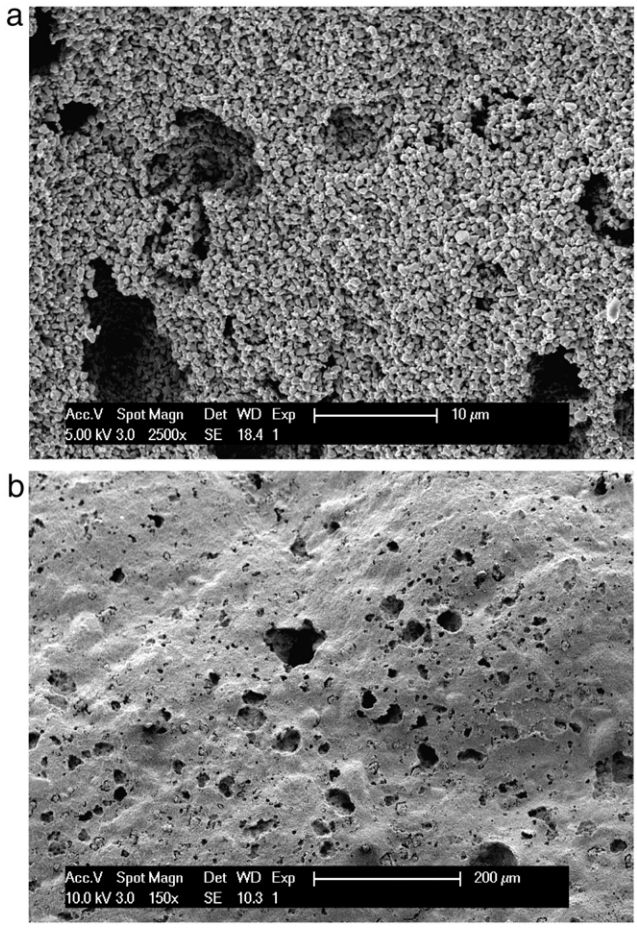

Fig. 8. Microstructure of presintered tubes, showing small pores with sizes of some μm (a) as well as big pores up to 100 μm (b).

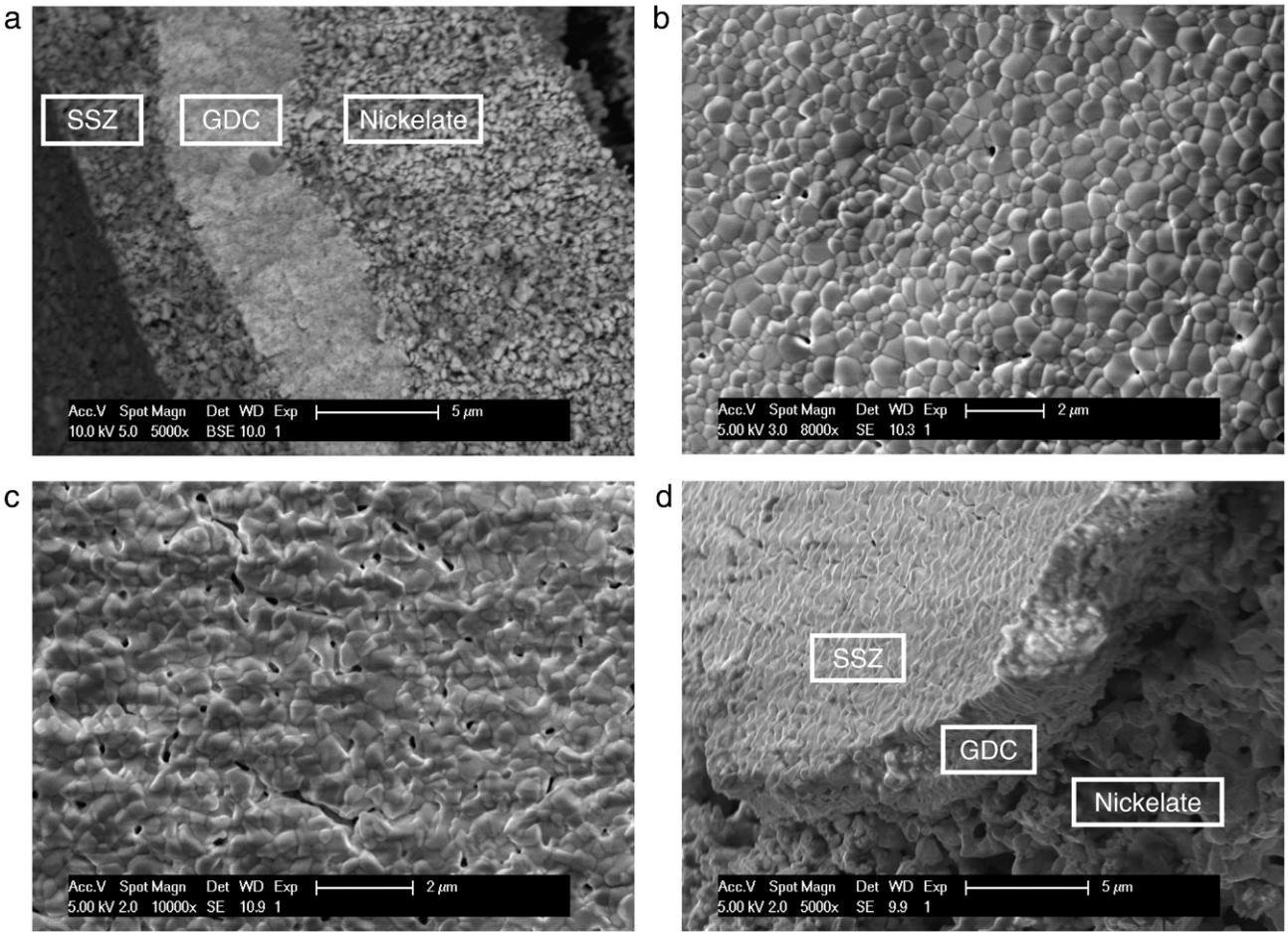

Fig. 9. SEM-images of dip-coated and dried nickelate, GDC and SSZ layers in the green state on presintered tubes. In the dried green state (a), films adhere well. After sintering, a topview on the GDC layer (b) shows a very dense microstructure. SSZ layer remains slightly porous after sintering, topview (c) and cross-section (d).

15% were necessary to densify GDC thin films. However, the powder particle size of GDC was 0.3 μm in contrast to $d_{v,50} = 0.18$ μm used in this study which can explain GDC densification despite the lower substrate shrinkage and highlights the importance of particle size for densification.

The densification of electrolyte layers at sintering temperatures as low as 1250 °C for GDC/SSZ bilayers is very encouraging. The nickelate layer, which is only applied to cover big pores, may be avoided when the surface state of the tubes is improved, which will simplify the processing. Investigations to optimise the pore size distribution of the cathode tubes, dip-coating parameters such as withdrawal speed and solid concentration of the suspensions, drying conditions and sintering temperatures as well as first power tests of complete cells are in progress.

4. Conclusion

The feasibility to produce cathode-supported SOFcells on porous nickelate substrates was demonstrated. Cathode-tubes of 4.9 mm inner diameter were fabricated by cold-isostatic pressing and presintering to 1060 °C. Electrolyte layers were applied by dip-coating and showed good densification after co-sintering. The densification of electrolyte layers was shifted to lower temperatures with attrition milling of their powders. Polyacrylic acid was used as dispersant for aqueous electrolyte suspensions and its required quantity defined by ζ-potential measurements. The next steps will be the fabrication and testing of complete cells as well as the optimisation of cathode tubes.

Acknowledgements

This study was financially supported by EPFL's Seed Fund of the Faculty of Engineering (STI).

References

[1] I.P. Kilbride, Journal of Power Sources 61 (1–2) (1996) 167.
[2] N.M. Sammes, Y.H. Du, International Journal of Applied Ceramic Technology 4 (2) (2007) 89.
[3] T.L. Nguyen, T. Honda, T. Kato, Y. Iimura, K. Kato, A. Negishi, K. Nozaki, M. Shiono, A. Kobayashi, K. Hosoda, Z.F. Cai, M. Dokiya, Journal of the Electrochemical Society 151 (8) (2004) A1230.
[4] P. Sarkar, L. Yamarte, H.S. Rho, L. Johanson, International Journal of Applied Ceramic Technology 4 (2) (2007) 103.
[5] Y. Funahashi, T. Shimamori, T. Suzuki, Y. Fujishiro, M. Awano, Journal of Power Sources 163 (2) (2007) 731.
[6] T. Suzuki, Y. Funahashi, T. Yamaguchi, Y. Fujishiro, M. Awano, Electrochemical and Solid-State Letters 10 (8) (2007) A177.
[7] T. Yamaguchi, S. Shimizu, T. Suzuki, Y. Fujishiro, M. Awano, Journal of the Electrochemical Society 155 (4) (2008) B423.
[8] Y. Liu, S.I. Hashimoto, H. Nishino, K. Takei, M. Mori, T. Suzuki, Y. Funahashi, Journal of Power Sources 174 (1) (2007) 95.
[9] Y. Liu, S.I. Hashimoto, K. Takei, M. Mori, Y. Funahashi, Journal of Fuel Cell Science and Technology 5 (3) (2008).
[10] T. Horita, N. Sakai, H. Yokokawa, M. Dokiya, T. Kawada, J. Van Herle, K. Sasaki, Journal of Electroceramics 1 (2) (1997) 155.
[11] J. Van herle, R. Ihringer, N.M. Sammes, G. Tompsett, K. Kendall, K. Yamada, C. Wen, T. Kawada, M. Ihara, J. Mizusaki, Solid State Ionics 132 (3–4) (2000) 333.
[12] S.J. Skinner, J.A. Kilner, Solid State Ionics 135 (1–4) (2000) 709.
[13] E. Boehm, J.M. Bassat, P. Dordor, F. Mauvy, J.C. Grenier, P. Stevens, Solid State Ionics 176 (37–38) (2005) 2717.
[14] C. Lalanne, G. Prosperi, J.M. Bassat, F. Mauvy, S. Fourcade, P. Stevens, M. Zahid, S. Diethelm, J. Van herle, J.C. Grenier, Journal of Power Sources 185 (2) (2008).

[15] F. Mauvy, C. Lalanne, S. Fourcade, J.M. Bassat, J.C. Grenier, Journal of the European Ceramic Society 27 (13–15) (2007) 3731.
[16] C. Lalanne, F. Mauvy, E. Siebert, M.L. Fontaine, J.M. Bassat, F. Ansart, P. Stevens, J.C. Grenier, Journal of the European Ceramic Society 27 (13–15) (2007) 4195.
[17] H.G. Pedersen, L. Bergstrom, Journal of the American Ceramic Society 82 (5) (1999) 1137.
[18] P. Bowen, C. Carry, D. Luxembourg, H. Hofmann, Powder Technology 157 (1–3) (2005) 100.
[19] U. Aschauer, Hamaker Lausanne (2008), http://ltp.epfl.ch/page65254.html.
[20] W.R. Bowen, F. Jenner, Advances in Colloid and Interface Science 56 (1995) 201.
[21] J. Gregory, Journal of Colloid and Interface Science 83 (1) (1981) 138.
[22] H. Ohshima, D.Y.C. Chan, T.W. Healy, L.R. White, Journal of Colloid and Interface Science 92 (1) (1983) 232.
[23] L. Bergstrom, C.H. Schilling, I.A. Aksay, Journal of the American Ceramic Society 75 (12) (1992) 3305.
[24] H. Hayashi, T. Saitou, N. Maruyama, H. Inaba, K. Kawamura, M. Mori, Solid State Ionics 176 (5–6) (2005) 613.
[25] M.Y. Gorshkov, N.M. Bogdanovich, A.D. Neuimin, L.A. Dunyushkina, A.V. Kuz'min, A.A. Pankratov, Russian Journal of Electrochemistry 43 (9) (2007) 987.
[26] T. Yamaguchi, T. Suzuki, S. Shimizu, Y. Fujishiro, M. Awano, Journal of Membrane Science 300 (1–2) (2007) 45.
[27] H. Hayashi, M. Kanoh, C.J. Quan, H. Inaba, S.R. Wang, M. Dokiya, H. Tagawa, Solid State Ionics 132 (3–4) (2000) 227.
[28] C.S. Montross, H. Yokokawa, M. Dokiya, British Ceramic Transactions 101 (2002) 85.
[29] L. Bergstrom, Advances in Colloid and Interface Science 70 (1997) 125.